Relationship between large-, meso, and small-scale field-aligned currents and their current carriers

M. YAMAUCHI, R. LUNDIN, and L. ELIASSON
IRF-Kiruna,
Box 812, S-98128 Kiruna, Sweden.

S. OHTANI
JHU/APL,
Johns Hopkins Road, Laurel, MD 20723-6099, U.S.A.

J. H. CLEMMONS
NASA/GSFC,
Greenbelt, MD 20771, U.S.A.

ABSTRACT. Carriers of the dayside large-scale field-aligned currents (FACs) are discussed. Since the gyro-radius of the current carriers are smaller than the size of small-scale FACs (a pair of upward and downward FACs associated with inverted-V potential structure as shown in Figure 1), the current carriers of large-scale FAC could be controlled by small-scale (and hence meso-scale) FACs. We restrict the discussion to only a few regions.

(1) Although the current carries are electrons in most cases, the framework of the large-scale FAC system is sometimes determined by positive ions, especially in the cusp.

(2) There is a dawn-dusk asymmetry in the relationship between the large-scale FACs and the current carriers. A substantial fraction of the Region-1 FAC is probably composed of many small-scale paired FACs which are associated with the inverted-V structure (see Figure 1), whereas the Region-2 FAC is carried by CPS electrons in the morning sector and by thermal electrons in the afternoon sector.

(3) Meso-scale FAC is formed by individual ion injections, but it has no relation to the large-scale FACs even inside the cusp region. Thus the large-scale cusp FACs (and the cusp itself) are formed by a steady mechanism but not by the meso-scale injections such is FTEs.. This rules out the FTE cusp model.

1. Introduction

The purpose of this study is to show low- and mid-altitude satellite observations of the field-aligned currents (FACs). Since Iijima and Potemra [1, 2] derived Region-1, Region-2, and cusp region (Region-0) large-scale FAC system from the satellite (TRIAD) magnetometer data, many observational efforts have been made on the subjects listed below. Some of them have been reviewed by Potemra [3].

1. Alternative means to derive FACs such as from ground geomagnetic disturbances, optical images, ionospheric convection patterns, and the electric fields [4-13; and references therein].

2. Distinguishing the wave and the real FACs [14-21; and references therein].

3. Seasonal variations [22-24; and references therein].

4. The current closure in the ionosphere [5, 8; and references therein].

5. Subdivision of the current system in terms of the source and behaviors (see review by Potemra [3] and references therein).

6. The distribution (shape, alignment, size) of each FAC regions [7, 23, 25-33; and references therein].

7. Macroscopic current carriers, i.e., relation to BPS, CPS, PSBL, cusp, cleft, and mantle. [16, 27, 31, 34-39; and references therein].

8. Microscopic current carriers, i.e., potential-accelerated aurora particles, black aurora, bursts, low-energy particles, and thermal particles [31, 40-44; and references therein].

9. The relation to small-scale and meso-scale FAC systems [13-16, 19, 45-47; and references therein].

10. The short-term development and long-term behavior in response to the change of external conditions [13, 23, 48-51; and references therein].

11. The current closure (source) in the magnetosphere.

All questions are of course further examined for various solar wind conditions and geomagnetic activities. Here, the term "meso-scale" simply means anything smaller than "regions" and larger than the inverted-V potential structures. For example, individual electron/ion energy-time dispersion and multiple injections are all meso-scale phenomena [46, 51, 52]. Compared to the first six questions (*1-6*), the next four questions (7-10) are rather poorly investigated and the available results are controversial and puzzling. The last question (*11*) has a large weight on the theoretical aspect, and lies outside the scope of this paper.

Thus, identifying the current carriers and revealing the cross-scale relations are the most needed topics. Here, we should note that Alfvén waves are related to both the conduction current (real) and the induction current (wave), and it is often impossible to distinguish wave (small and meso scales) or conduction current (meso and large scales) for the stationary Alfvén structure [53, 54]. The same problem occurs for the electrostatic shocks and weak double layers which are associated with cavitons [31, 55]. Obvious questions related to the current carriers are: (a) carrier species (ion or electron); (b) energy of the carrier; and (c) their energization mechanisms, e.g., the parallel electric potential, waves (burst), thermalization, Fermi-acceleration, and J x B force. The answers to these questions depend on the location (MLT/latitude), altitude, and the scale-size of the FAC system. For example, the current carrier can be different between the morning side Region-1 FAC, near-noon downward FAC, afternoon Region-2 FAC, and substorm-related downward FAC, although it has been generally assumed that upward FACs are carried by auroral electrons whereas downward FACs are carried by ionospheric thermal electrons. It is impossible to cover all the aspects of current-carrier problem, and we show only a few observations of the dayside FAC system.

2. Relation Between Large-scale FACs and Small-scale FACs

The large-scale FACs often contain many upward and downward pairs of small-scale FACs [14, 15, 19]. It is a question whether these small-scale FACs are simply added to the background large-scale FACs, or the difference of the upward and downward small-scale FACs makes up the large-scale FACs. In the former case, the large-scale FACs are basically carried by the thermal electrons and are independent of the small-scale FACs of the Alfvén waves. In the latter case a substantial portion of the small-scale FACs must be a stationary structure (such as the electrostatic shocks and weak double layers [19]) and the current carriers are not necessarily the thermal electrons. It has been generally believed that small-scale FACs are induction currents of Alfvén waves and therefore they cannot form the large-scale FACs.
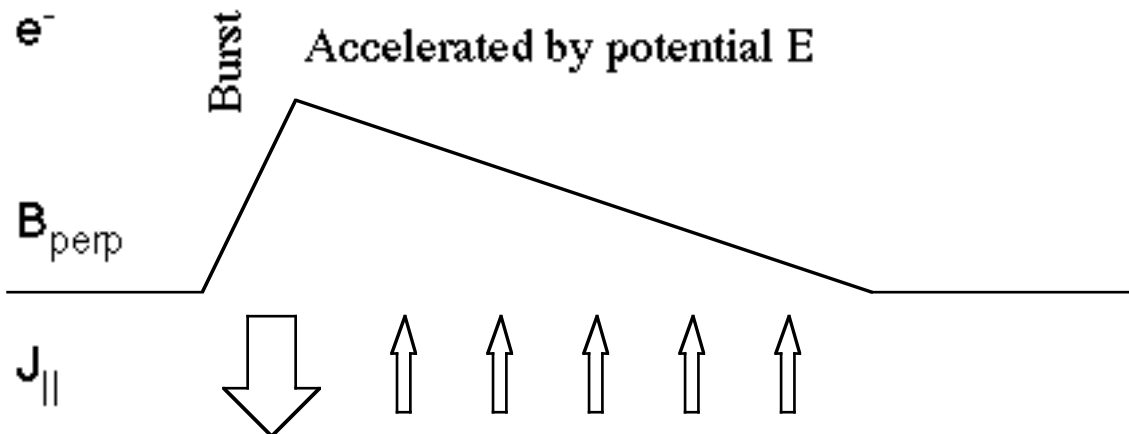

Figure 1. Relative strength and carriers of small-scale FACs in the night-side sector.

However, FREJA [31] and FAST [44] satellites revealed that many FAC spikes in the night-side sector are associated with electron bursts and field-aligned potential drops as shown in Figure 1. They are of the small-scale, but yet stationary structure associated with the ionospheric plasma cavities [31, 55]. This structure is often denoted the electrostatic shocks. The observations are made at a few thousand km altitude, and the picture is altitude-dependent [R. Ergun, private communication, 1997]. Burch *et al.* [42] using DE-1 data at mid-altitude concluded that 20-200 eV upward electrons are the major carriers of the downward FAC near the cusp. Although they concluded that electric potential causes an energization of upward electrons (carriers of downward FAC), the observation itself generally agrees with the above view, i.e., the energetic electrons are not necessarily accelerated by a potential electric field but by the waves. Therefore, we have to consider this type of FAC carriers (Figure 1) as well as the traditional thermal electrons and precipitating auroral electrons [40, 41].

Now we have the following questions: How should we understand these small-scale stationary FACs in the framework of large-scale FACs? What portion of the FAC is carried by energized electrons and what portion by thermal electrons? This is not a

simple question because the same types of plasma population (CPS, BPS, LLBL, cusp, cleft, etc. [56-59; and references therein]) must explain the opposite sense of FACs between dawn and dusk. For example, we have to associate the CPS plasma population to both upward (dawn) and downward (dusk) Region-2 FACs, whereas the BPS or LLBL plasma population must explain downward (dawn) and upward (dusk) Region-1 FACs.

2.1. MORNING SECTOR

We start with the dawnside FACs. The small-scale FAC of Figure 1 has some similarity to Region-1 and Region-2 FACs: the downward FAC is associated with a bursty electron region (this is the characteristics of BPS and LLBL), whereas the upward FAC is associated with a weak potential drop (this is the characteristic of CPS because of the mirror force [60, 61]). Figure 2 shows one such example [43]. Nearly 40% of the Region-1 FAC is concentrated within a tiny region of a spike-like FAC at around 21:35 UT, which is accompanied by the upward electron burst of BPS.

Figure 2. Particle and magnetic field data from Viking orbit 176 (25 March, 1986). Positive (negative) slopes of B_E mean upward (downward) FACs. Region-1 FAC is found at around 74°-75° Inv., and Region-2 FAC is found at around 72°-73° Inv. (after [43]).

Figure 3. Particle and magnetic field data from Freja orbit 2388 (5 April, 1993). Positive (negative) slopes of B_E mean upward (downward) FACs at 17 MLT, and positive (negative) slopes of B_N mean upward (downward) FACs at 13 MLT. Corresponding to cusp, BPS, and CPS, we find cusp region FACs, upward Region-1 FAC, and Region-2 FAC, respectively.

On the other hand, 60% of the downward FAC are not associated with energized electrons. This need further investigation because VIKING could have missed the small-scale electron bursts if the scale size of the electron burst is smaller than the time resolution of VIKING which detects upward electrons only once every 20 seconds (spin period). For example, the ion conics which is seen all the way from 21:31 UT to 21:36 UT indicates waves activities and possible electron burst in this region. Therefore, we can conclude only that some portion of downward Region 1 FAC is composed of upward electron burst associated with the electrostatic shocks (and cavitons), but contributions from the thermal electrons are still unknown. None of the past studies give sufficient answer to this.

All Region-2 FACs are found in the region of CPS particles. Except for its poleward boundary where CPS electrons and BPS electrons coexist, we do not find any electron bursts below 73° Inv. The large-scale FAC in this part is not the sum of the small-scale paired FACs, but is carried by the precipitating CPS electrons accelerated

by the large-scale steady electrostatic potential structure. This is consistent with previous results [40, 41]. However, its poleward part (21:38-21:39 UT) is different. It is apparently composed of many paired FACs which agrees with the small-scale structures shown in Figure 1 or the meso-scale magnetic fluctuations associated with Pc 4-5 pulsations [16] and/or transient magnetosheath plasma injections (PTE) [46] inside CPS. According to the total magnetic deviation, this part contributes about 50% of the total upward Region-2 FAC. The question is if the FAC in this part is contributed by such small- (or meso-)scale FACs. The majority of FAC in this region could still be carried by thermal electrons if the small- (meso-)scale FACs adds only minor spikes (up and down) without net FACs. Since the FAC regions are determined simply by its sense (upward or downward), one may not draw a general conclusion on the co-existing population without thorough statistics. Yet we see some cases of Region-2 FACs without any small-scale spikes related to the electrostatic shocks (e.g., Figure 1 of [38]). So, we may at least conclude that CPS-related upward FACs are carried by these CPS electrons and are not the sum of small-scale FACs. Contribution from the small-scale FACs to the dawnside Region-2 FAC is a future problem.

2.2. AFTERNOON SECTOR

Let us move to the dusk sector. BPS electrons are now associated with the inverted-V structures, discrete aurora, and upward FACs. The relation is self-consistent. However, we have a puzzle concerning the CPS-related Region 2 FAC. It flows downward, i.e., the current carriers (electrons) must move upward whereas the plasma regime in this region (CPS) is in favour of upward FACs (cf. morning sector). So, we have to find a different type current carrier in this region.

Figure 3 shows the FREJA particle and magnetic field observations in the noon and dusk sectors. The satellite traversed the BPS region and CPS region at around 00:40 UT. Region-1 and Region-2 FACs are found exactly in the BPS and CPS regions, respectively. Enlarged plots of the electron data [62] in these regions are shown in Figure 4. Figure 4a (BPS = upward FAC) clearly shows intermittent inverted-V potential structures, indicating that the Region-1 FAC is subdivided into many small-scale FACs as is expected. However, the upward electron burst (expected in Figure 1) is barely seen. Certainly, the small-scale FAC structures are quite different between dawn and dusk. We instead see upward low-energy electrons (< 70 eV) continuously. The same type of upward low-energy electrons extends to the CPS region as is clear from Figure 4b. These electrons must be the carriers for the downward FAC, and hence Region-2 FAC may not be divided into small-scale FACs contrary to Region-1 FAC.

In summary, the relation between the large-scale and the small-scale FACs is similar in both sectors. The major differences between dawn and dusk are the roles of thermal electrons and electron burst. Contributions to the FACs are largest from the auroral precipitating electron (upward FAC), the second largest from the low-energy upward electrons (downward FAC), the third largest from the CPS-origin precipitating electrons (upward FACs), and barely from electron burst (downward FAC). The majority of upward FAC in the BPS is associated with intermittent inverted-V structures and the majority of the downward FAC in the CPS is carried by low-energy electrons .

2.3. NOON SECTOR

Obtaining the current carrier is more difficult because the cusp is normally filled with various wave activities [63], which makes it difficult to identify the electron population. Burch *et al*. [42] showed that at mid-altitude upward electron beams can explain the cusp Region-1 FAC in the prenoon sector, but the situation is not so simple. Electron data for the cusp part in Figure 3 is enlarged in Figure 5. There is no difference between the upward FAC region and the downward FAC region. Both regions are filled with supra-thermal electron bursts and the injecting electrons. Ion conics and beams [64] are another possible clue, because the ion beams usually indicate inverted-V potential structure below the satellite whereas ion conics usually indicate wave activity below the satellite (same source for the electron burst). However, we again find a lack of good correlation between the ion beams/conics and the senses (upward/downward) of FACs. Apparently the cusp large-scale FAC is not a simple extension of the dawnside/duskside Region-1 or Region-2 FACs [4, 27, 33, 36, 37]. This is one of the counter-evidence against the reconnection-related cusp models, e.g., by Cowley *et al*. [65; and references therein].

Figure 4. High-resolution electron data of Figure 3: (a) BPS part (upward Region-1 FAC); (b) CPS part (downward Region-2 FAC). The upper two panels in each figures show downward field-aligned electrons, the third panel shows trapped electrons (90° pitch angle), and the last panel shows upward field-aligned electrons.

Figure 5. High-resolution electron data for the cusp part of Figure 3: (a) upward FAC region; (b) downward FAC region. The format is the same as Figure 4.
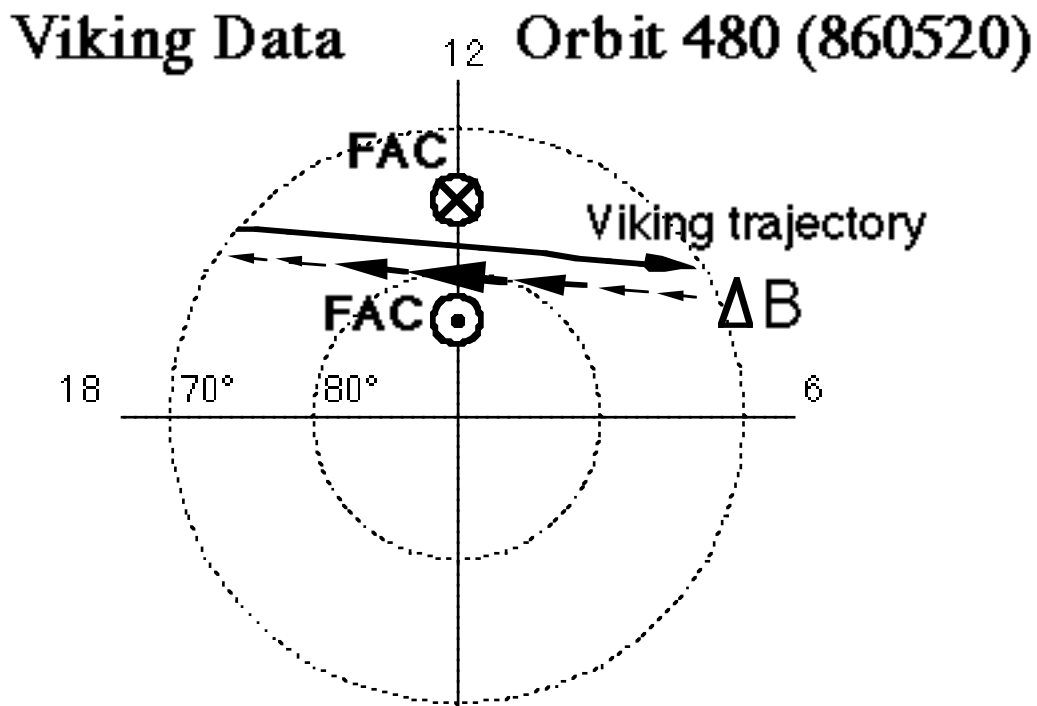
Figure 6. Particle and magnetic field data from Viking orbit 480 (20 May, 1986). Positive (negative) slopes of B_N mean downward (upward) FACs. Positive deviation B_N indicates upward FAC poleward of the satellite and/or downward FAC equatorward of the satellite [45].

3. Relation Between Large-scale FACs and Meso-scale FACs

Although we do not see a clear signature of meso-scale FAC systems in Figures 2 and 3, they are often observed in the dawn and dusk sectors together with transient plasma injections (PTE) and/or Pc 4-5 pulsations as mentioned above [16, 46]. These meso-scale FACs usually have bipolar signatures. So, it is difficult to estimate their contribution to Region-2 FAC. Region-2 FAC always exists in the CPS regardless of the existence of such meso-scale FACs. The same type of semi-independence is seen for the travelling convection vortices [66]. Relations between PTE and TCV are under investigation. Only the exception for such independence between the meso-scale FAC and the large-scale FAC could be the series of auroral spots at 14-15 MLT [13, 67, and references therein]: the meso-scale FACs may form the large-scale Region-1 and Region-2 FACs there. But, these meso-scale FACs are smaller in intensity than the cusp FAC. In Figure 3, the first large bipolar signature of B_N is the cusp FAC but all the other minor bipolar signatures and ion injections near 14-15 MLT are probably the LLBL-related afternoon auroral spots.

What about the cusp? Yamauchi and Lundin [52] showed that cusp is generally composed of many meso-scale plasma injections. Individual injection often carries a pair of FAC [39, 45]. However, the amount of the current carried by the individual injection is far below the large-scale cusp FACs. Figure 6 (after [45], their Figure 15) shows one example. IMF is strongly duskward (By = + 5 nT); i.e., upward FACs must be located poleward of the cusp and downward FAC equatorward of the cusp. Such FACs are easily verified by the B_E deviation. The meso-scale FACs are deduced from B_N. It is well correlated with the magnetosheath plasma injections but is nevertheless not forming the large-scale cusp-region FACs. The same result is obtained by the FREJA satellite [39]. The result argues against FTE-related cusp models [68, 69] in which the entire large-scale cusp region FAC is composed of meso-scale FACs.

Yet, meso-scale FACs carried by the meso-scale plasma injections could be important in the formation of the cusp FAC. Although such studies are difficult with single satellite observations because of the separation problem between the temporal development and the spatial structure, Yamauchi et al. [51] showed a clear case when the IMF turned from steady southward to steady northward. The cusp current flows in the cusp part, but some meso-scale FAC is also found in the equatorward injection. The observation indicates that either the cusp is moving back and forth, or we have an independent meso-scale injection. All the above observations support the wave-assisted cusp model by Yamauchi and Lundin [70; and references therin]. The unusual observation of the meso-scale injections and FACs equatorward of the steady cusp during northward IMF [71] could belong to such a category although the injection could be attributed to the plasma transfer event [72]. Note that some of the meso-scale magnetosheath plasma injections into the low-altitude CPS region do not accompany FACs at all [73], indicating that they are not FTEs that Southwood has modelled [74].

The cusp region FACs are somewhat troublesome. Although the plasma regime (ion) clearly determines the entire region of large-scale FAC, the shape of FAC regions is unclear. In Figure 3, the magnetic deviation in the cusp region is seen mainly in the

north-south component of the magnetic field, indicating that the current system is aligned in the north-south direction. However, Figure 6 shows the opposite. In both cases the satellite traversed the cusp azimuthally.

4. Summary

It is yet too early for far-reaching conclusions without thorough statistics. Here we just list some summaries of several case studies.

The Region-1 and 2 FACs are well located in BPS/LLBL and CPS, respectively, in both the dawn and dusk sectors. This fact naturally causes some asymmetry of the current carrier between the dawn and dusk. The dawn Region-2 FAC is mostly carried by CPS electrons precipitating into the ionosphere whereas the duskside Region-2 FAC is carried by ionospheric low-energy (mostly thermal) electrons. The current carriers in the Region-1 FAC could be symmetric if it is mostly composed of many small-scale FACs as shown in Figure 1. However, its fine structure is different between dawn and dusk because the upward small-scale FACs inside an inverted-V potential structure is wide-spread compared to the downward small-scale FACs which are carried by the bursty electrons next to the inverted-V structure. Furthermore, the upward electron burst does not necessarily exist in the duskside Region-1 FAC. The roles of the thermal electron for the dawnside Region-1 FAC and of small- and meso-scale FACs for the dawnside Region-2 FAC must be investigated in the future.

The cusp FACs are not well understood. Meso-scale FACs are related with individual plasma injections, but unlike these injections, the meso-scale FACs do not constitute the large-scale FACs. They add minor bipolar signatures to the steady large-scale current system. The current carriers are quite unknown in the cusp region. We need thorough statistics, and any studies from a limited data set are not sufficient to solve the current carrier problem in the cusp region.
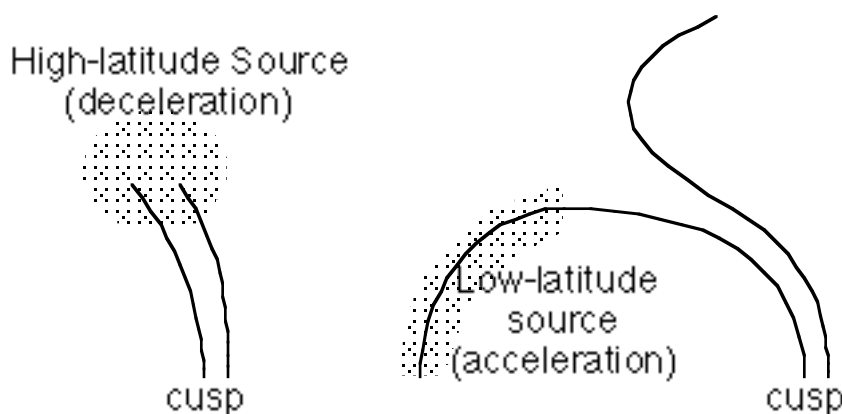
Figure 7. Proposed locations of the cusp (region-1) FAC. If the source is high-latitude, the decelerated solar wind directly drives a dynamo [76, 77]. If the source is low-latitude, the solar wind is accelerated and energy must come somewhere else. In this case, the cusp region-1 FAC must be dispersed and weak compared to cusp region-0 FAC, which is against the observation.

5. Restriction in Modelling

Before closing this rather diagnostic paper, let us mention some important notes for modelling. Since the FAC is a sink or a source of energy, any 2-D model needs an additional sink and source as the 3rd dimension effect [75-77]. For instance, the FAC transports energy from the source region to the ionosphere.

One may classify the source into two types: (1) constant dynamo (deceleration of convection or solar wind) and (2) constant total energy (conversion of "stored" electromagnetic energy). If the flow (e.g., solar wind) is steady, the former system predicts a long-term development of FAC toward a steady value whereas the latter predicts a decay of FAC system due to the ionospheric joule dissipation. According to MAGSAT observations, the cusp FAC system is quite steady and never decays [23]. So, the FAC system must take energy from the solar wind (decelerate the solar wind somewhere) rather than from the "stored" magnetic field. Next question is the location of dynamo; i.e., poleward of the cusp (cusp region-0 FAC) or equatorward of the cusp (cusp region-1 FAC). During southward IMF, the equatorward FAC is always stronger than the poleward FAC, indicating that the dynamo is connected to the cusp region-1 FAC rather than the cusp region-0 FAC (mantle FAC). This gives us a restriction in mapping the FAC system, as shown in Figure 7 because the solar wind must be decelerated in the source region. Apparently, we have to map the cusp to the high-latitude dynamo region [70, 76] rather than the dayside magnetopause [78, 79]. The same conclusion is also obtained from the high-altitude observations of the cusp by HAWKEYE [80, 81], INTERBALL [82], and POLAR [83] spacecrafts. One may not simply map the low-altitude FAC beyond the high-altitude cusp [84, 85].

6. References

1. Iijima, T. and Potemra, T.A. (1976a) The amplitude distribution of field-aligned currents at northern high latitudes observed by Triad, *J. Geophys. Res.* **81**, 2165.
2. Iijima, T. and Potemra, T.A. (1976b) Field-aligned currents in the dayside cusp observed by Triad, *J. Geophys. Res.* **81**, 5971-5979.
3. Potemra, T.A. (1994) Sources of large-scale Birkeland currents, in J.A. Holtet and A. Egeland (eds.), *Physical signatures of magnetospheric boundary layer process*, Kluwer Academic Publishers, Dordrecht, pp. 3-27.
4. Akasofu, S.-I. (1977) *Physics of magnetospheric substorms*, Reidel.
5. Wilhjelm, J., Friis-Christensen, E., and Potemra, T.A. (1978) The relationship between ionospheric and field-aligned currents in the dayside cusp, *J. Geophys. Res.* **83**, 5586-5594.

6. Brekke, A., Doupnik, J.R., and Banks, P.M. (1974) Incoherent scatter measurements of E region conductivities and currents in the auroral zone, *J. Geophys. Res.* **79**, 3773-3790.

7. Levitin, A.E., Afonina, R.G., Belov, B.A., and Feldstein, Y.I. (1982) Geomagnetic variation and field-aligned currents at northern high-latitudes, and their relationship to the solar wind parameters, *Phil. Trans. R. Soc. Lond.* **A304**, 253-301.

8. Friis-Christensen, E., Kamide, Y., Richmond, A.D., and Matsushita, S. (1985) Interplanetary magnetic field control of high-latitude electric fields and currents determined from Greenland magnetometer data, *J. Geophys. Res.* **90**, 1325-1338.

9. Feldstein, Y.I. and Galperin, Yu.I. (1985) The auroral luminosity structure in the high-latitude upper atmosphere: its dynamics and relationship to the large-scale structure of the earth's magnetosphere, *Rev. Geophys.* **23**, 217.

10. Burch, J.L., Reiff, P.H., Menietti, J.D., Heelis, R.A., Hanson, W.B., Shawhan, S.D., Shelley, E.G., Sugiura, M., Weimer, D.R., and Winningham, J.D. (1985) IMF B_Y dependent plasma flow and birkeland currents in the dayside magnetosphere 1. dynamics explorer observations, *J. Geophys. Res.* **90**, 1577-1593.

11. Heppner, J.P. and Maynard, N.C. (1987) Empirical high-latitude electric field models, *J. Geophys. Res.* **92**, 4467-4489.

12. Blomberg, L.G. and Marklund, G.T. (1991) High-latitude convection patterns for various large-scale field-aligned current configurations, *Geophys. Res. Lett.* **18**, 717-720.

13. Elphinstone, R.D., Hearn, D., Murphree, J.S., Cogger, L.L., Johnson, M.L., and Vo, H.B. (1993) Some UV dayside auroral morphologies, in *Auroral Plasma Dynamics*, American Geophysical Union, Washington, 31-45.

14. Sugiura, M. (1984) A fundamental magnetosphere-ionosphere coupling mode involving field-aligned currents as deduced from DE-2 observations, *Geophys. Res. Lett.* **11**, 877-880.

15. Weimer, D.R., Goertz, C.K., Gurnnet, D.A., Maynard, N.C., and Burch, J.L. (1985) Auroral zone electric fields from DE 1 and 2 at magnetic conjunctions, *J. Geophys. Res.* **90**, 7479.

16. Potemra, T.A., Zanetti, L.J., Bythrow, P.F., Erlandson, R.E., Lundin, R., Marklund, G.T., Block, L.P. and Lindqvist, P.-A. (1988) Resonant geomagnetic field oscillations and Birkeland currents in the morning sector, *J. Geophys. Res.* **93**, 2661-2674.

17. Ishii, M., Sugiura, M., Iyemori, T., and Slavin, J.A. (1992) Correlation between magnetic and electric fields in the field-aligned current regions deduced from DE-2 observations, *J. Geophys. Res.* **97**, 13877.

18. Knudsen, D.J., Kelley, M.C., and Vickerey, J.F. (1992) Alfvén waves in the auroral ionosphere: A numerical model compared with measurement, *J. Geophys. Res.* **97**, 77.

19. Marklund, G. (1993) Viking investigations of auroral electrodynamical processes, J. Geophys. Res., 98, 1691-1704, 1993.

20. Peterson, W.K., Abe, T., André, M., Engebretson, M.J., Fukunishi, H., Hayakawa, H., Matsuoka, A., Mukai, T. Persoon, A.M., Retterer, J.M., Robinson, R.M., Sugiura, M., Tsuruda, K., Wallis, D.D., and Yau, A.W. (1993) Observations of a

transverse magnetic field perturbation at two altitudes on the equatorward edge of the magnetospheric cusp, *J. Geophys. Res.* **98**, 21463-21470.

21. Lühr, H., Warnecke, J., Zanetti, L.J., Lindqvist, P.A., and Hughes, T.J. (1994) Fine structure of field-aligned current sheets deduced from spacecraft and ground-based observations: Initial Freja results, *Geophys. Res. Lett.* **21**, 1883-1886.

22. Fujii, R. and Iijima, T. (1987) The control of the ionospheric conductivities on large-scale birkeland current intensities under geomagnetic quiet conditions, *J. Geophys. Res.* **92**, 4505-4513.

23. Yamauchi, M. and Araki, T. (1989) The interplanetary magnetic field B_Y-dependent field-aligned current in the dayside polar cap under quiet conditions, *J. Geophys. Res.* **94**, 2684-2690.

24. Lu, G., Richmond, A.D., Emery, B.A. Reiff,, P.H., de la Beaujardiere, O., Rich, F.J., Denig, W.F., Kroehl, H.W., Lyons, L.R., Ruohoniemi, J.M., Friis-Christensen, E., Opgenoorth, H., Persson, M.A.L., Lepping, R.P., Rodger, A.S., Hughes, T., McEwin, A., Dennis, S., Morris, R., Burns, G., and Tomlinson, L. (1994) Interhemispheric asymmetry of the high-latitude ionospheric convection pattern, *J. Geophys. Res.* **99**, 6491-6510.

25. Kamide, Y., Craven, J.D., Frank, L.A., Ahn, B.-H., and Akasofu, S.-I. (1986) Modeling substorm current systems using conductivity distributions inferred from DE auroral images, *J. Geophys. Res.* **91**, 11235-11256.

26. Iijima, T. and Shibaji, T. (1987) Global characteristics of northward IMF-associated (NBZ) field-aligned currents, *J. Geophys. Res.* **92**, 2408-2424.

27. Erlandson, R.E., Zanetti, L.J., Potemra, T.A., Bythrow, P.F., and Lundin, R. (1988) IMF B_Y dependence of region 1 birkeland currents near noon, *J. Geophys. Res.* **93**, 9804-9814.

28. Hoffman, R.A., Sugiura, M., Maynard, N.C., Candey, R.M., Craven, J.D., and Frank, L.A. (1988) Electrodynamic patterns in the polar region during periods of extreme magnetic quiescence, *J. Geophys. Res.* **93**, 14515-14541.

29. Murphree, J.S., Johnson, M.L., Cogger, L.L., and Hearn, D.J. (1994) Freja UV imager observations of spatially periodic auroral distortions, *Geophys. Res. Lett.* **21**, 1887-1890.

30. Yamauchi, M., Lundin, R., and Aparicio, B. (1992) Viking observation of the substorm current wedge, *ESA SP* **335**, 495-497.

31. Marklund, G., Blomberg, L., Fälthammar, C.-G., and Lindqvist, P.-A. (1994) On the diverging electric fields associated with black aurora, *Geophys. Res. Lett.* **21**, 1859-1962.

32. Ohtani, S., Zanetti, L.J., Potemra, T.A., Baker, K.B., Ruohoniemi, J.M., and Lui, A.T.Y. (1994) Periodic longitudinal structure of field-aligned currents in the dawn sector: large-scale meandering of an auroral electrojet, *Geophys. Res. Lett.* **21**, 1879-1882.

33. Ohtani, S., Potemra, T.A., Newell, P.T., Zanetti, L.J., Iijima, T., Watanabe, M., Yamauchi, M., Elphinstone, R.D., de la Beaujardiere, O., and Blomberg, L.G. (1995) Simultaneous prenoon and postnoon observations of three field-aligned current systems from Viking and DMSP-F7, *J. Geophys. Res.* **100**, 119-136.

34. McDiarmid, I.B., Burrows, J.R., and Wilson, M.D. (1979) Large-scale magnetic field perturbations and particle measurements at 1400 km on the dayside, *J. Geophys. Res.* **84**, 1431-1441.

35. Bythrow, P.F., Potemra, T.A., and Hoffman, R.A. (1982) Observations of field-aligned currents, particles, and plasma drift in the polar cusps near solstice, *J. Geophys. Res.* **87**, 5131-5139.

36. Bythrow, P.F., Potemra, T.A., Erlandson, R.E., Zanetti, L.J., and M. Klumpar, D. (1988) Birkeland currents and charged particles in the high-latitude prenoon region: A new interpretation, *J. Geophys. Res.* **93**, 9791-9803.

37. Yamauchi, M., Lundin, R., and Woch, J. (1993a) The interplanetary magnetic field By effects on large-scale field-aligned currents near local noon: Contributions from cusp part and noncusp part, *J. Geophys. Res.* **98**, 5761-5767.

38. Woch, J., Yamauchi, M., Lundin, R., Potemra, T.A., and Zanetti, L.J. (1993) The low-latitude boundary layer at mid-altitudes: Relation to large-scale Birkeland currents, *Geophys. Res. Lett.* **20**, 2251-2254.

39. Andersson, L., Nilsson, H., and Wahlund, J.-E. (1997) Meso-scale structure in the cusp/cleft region, *Phys. Chem. Earth*, 22, 663-667.

40. Anderson, H.R. and Vondrak, R.R. (1975) Observations of Birkeland currents at auroral latitudes, *Rev. Geophys. Space Phy.* **13**, 243.

41. Klupmar, D.M. (1979) Relationships between auroral particle distributions and magnetic field perturbations associated with field-aligned currents, *J. Geophys. Res.* **84**, 6524-6532.

42. Burch, J.L., Reiff, P.H., and Sugiura, M. (1983) Upward electron beams measured by DE-1: a primary source of dayside region-1 birkeland currents, *Geophys. Res. Lett.* **10**, 753-756.

43. Potemra, T.A., Zanetti, L.J., Erlandson, R.E., Bythrow, P.F., Gustafsson, G., Acuna, M.H., and Lundin, R. (1987) Observations of large-scale Birkeland currents with Viking, *Goephys. Res. Lett.* **14**, 419-422.

44. Ergun, R.E., Carlson, C.W., McFadden, J.P., Chaston, C., Delory, G.T., Peria, W., Mozer, F.S., Temerin, M., Elphic, R., Strangeway, R., Klumpar, D.M., Shelley, E.G., Peterson, W.K., Moebius, E., Kistler, L., Cattell, C., and Pfaff, R. (1997) Initial results from the FAST satellite: Solitary waves and AKR, *Ann. Geophys.* **15** *Sup.*, 683.

45. Lundin, R., Woch, J., and Yamauchi, M. (1991) The present understanding of the cusp, *ESA SP* 330 83-95.

46. Woch, J. and Lundin, R. (1992) Signature of transient boundary layer processes observed with Viking, *J. Geophys. Res.* **97**, 1431-1447.

47. Ohtani, S., Blomberg, L.G., Newell, P.T., Yamauchi, M., Potemra, T.A., and Zanetti, L.J. (1996) Altitudinal comparison of dayside field-aligned current signatures by Viking and DMSP-F7: Intermediate-scale FAC systems, *J. Geophys. Res.* **101**, 15297-15310.

48. Primdahl, F. and Spangslev, F. (1983) Does IMF By induce the cusp field-aligned current? *Planet. Space Sci.* **31**, 363-367.

49. Clauer, C.R. and Banks, P.M. (1986) Relationship of the interplanetary electric field to the high-latitude ionospheric electric field and currents: Observations and model simulation, *J. Geophys. Res.* **91**, 6959-6971.

50. Knipp, D.J., Richmond, A.D., Emery, B., Crooker, N.U., de la Beaujardiere, O., Evans, D., and Kroehl, H. (1991) Ionospheric convection response to changing IMF direction, *Geophys. Res. Lett.* **18**, 721-724.

51. Yamauchi M., Lundin, R., and Potemra, T. (1995) Dynamic response of the cusp morphology to the IMF changes: An example observed by Viking, *J. Geophys. Res.* **100**, 7661-7670.

52. Yamauchi, M. and Lundin, R. (1994) Classification of large-scale and meso-scale ion dispersion patterns observed by Viking over the cusp-mantle region, in J.A. Holtet and A. Egeland (eds.), *Physical signatures of magnetospheric boundary layer process*, Kluwer Academic Publishers, Dordrecht, pp. 99-109.

53. Goertz, C.K. (1984) Kinetic Alfvén waves on auroral filed lines, *Planet. Space Sci.* **32**, 1387-1392.

54. Lysak, R.L. (1997) Propagation of Alfvén waves through the ionosphere, *Phys. Chem. Earth,* in press.

55. Lundin, R., Eliasson, L., Haerendel, G., Boehm, M., and Holback, B. (1994) Large-scale auroral plasma density cavities observed by Freja, *Geophys. Res. Lett.* **21**, 1903-1906.

56. Winningham, D.J., Yasuhara, F., Akasofu, S.-I., and Heikkila, W.J. (1975) The latitudinal morphology of 10 eV to 10 keV electron fluxes during quiet and disturbed times in the 2100-0300 MLT sector, *J. Geophys. Res.* **80**, 3148.

57. Kremser, G. and Lundin, R. (1990) Average spatial distributions of energetic particles in the midaltitude cusp/cleft region observed by Viking, *J. Geophys. Res.* **95**, 5753-5766.

58. Newell, P.T. and Meng, C.-I. (1992) Mapping the dayside ionosphere to the magnetosphere according to particle precipitation characteristics, *Geophys. Res. Lett.* **19**, 609-612.

59. Woch, J. and Lundin, R. (1993) The low-latitude boundary layer at mid-altitudes: Identification based on Viking hot plasma data, *Geophys. Res. Lett.* **20**, 979-982.

60. Alfvén, H. and Fälthammar, C.G. (1963) *Cosmical Electrodynamics*, Fundamental Principles, Clarendon, Oxford.

61. Fridman, M. and Lemaire, J. (1980) Relationship between auroral electron fluxes and field-aligned electric potential difference, *J. Geophys. Res.* **85**, 664.

62. Boehm, M., Paschmann, G., Clemmons, J., Höfner, H., Fremzel, R., Ertl, M., Haerendel, G., Hill, P., Lauche, H., Eliasson, L., and Lundin, R. (1994) The TESP electron spectrometer and correlator (F7) on Freja, *Space Sci. Rev.* **70**, 509-540.

63. Pottelette, R., Malingre, M., Dubouloz, N., Aparicio, B., Lundin, R., Holmgren, G., and Marklund, G. (1990) High-frequency waves in the cusp/cleft regions, *J. Geophys. Res.* **95**, 5957-5971.

64. Thelin, B. and Lundin, R. (1990) Upflowing ionospheric ions and electrons in the cusp-cleft region, *J. Geomag. Geoelectr.* **42**, 753-761.

65. Cowley, S.W.H., Morelli, J.P., and Lockwood, M. (1991) Dependence of convective flows and particle precipitation in the high-latitude dayside ionosphere on the X and Y components of the interplanetary magnetic field, *J. Geophys. Res.* **96**, 5557-5564.

66. Friis-Christensen, E., McHenry, M.A., Clauer, C.R., and Vennerstrom, S. (1988) Ionospheric traveling convection vortices observed near the polar cleft: a triggered response to sudden changes in the solar wind, *Geophys. Res. Lett.* **15**, 253-256.

67. Lundin, R., Yamauchi, M., Woch, J., and Marklund, G. (1995) Boundary layer polarization and voltage in the 14 MLT region, *J. Geophys. Res.* **100**, 7587-7597.

68. Smith, M.F. and Lockwood, M. (1990) The pulsating cusp, *Geophys. Res. Lett.* **17**, 1069-1072.

69. Lockwood, M. (1994) Ionospheric signatures of pulsed magnetopause reconnection, in J.A. Holtet and A. Egeland (eds.), *Physical signatures of magnetospheric boundary layer process*, Kluwer Academic Publishers, Dordrecht, pp. 229-243.

70. Yamauchi, M. and Lundin, R. (1997) The wave-assisted cusp model: comparison to low-altitude observations, *Phys. Chem. Earth*, 22, 729-734.

71. Potemra, T.A., Erlandson, R.E., Zanetti, L.J., Arnordy, R.L., Woch, J., and Friis-Christensen, E. (1992) The dynamic cusp, *J. Geophys. Res.* **97**, 2835-2844.

72. Lemaire, J. (1977) Impulsive penetration of filamentary plasma elements into the magnetospheres of the Earth and Jupiter, *Planet. Space Sci.* **25**, 887-890.

73 Yamauchi, M., Woch, J., Lundin, R., Shapshak, M., and Elphinstone, R. (1993b) A new type of ion injection event observed by Viking, *Geophys. Res. Lett.* **20**, 795-798.

74. Southwood, D.J. (1987) The ionospheric signature of flux transfer event, *J. Geophys. Res.* **92**, 3207.

75. Sato, T. and Iijima, T. (1979) Primary sources of large-scale Birkeland current, *Space Sci. Rev.* **24**, 347-366.

76. Yamauchi, M., Lundin, R., and Lui, A.T.Y. (1993c) Vorticity equation for MHD fast waves in geospace environment, *J. Geophys. Res.* **98**, 13523-13528.

77. Yamauchi, M. (1994) Numerical simulation of large-scale field-aligned current generation from finite-amplitude magnetosonic waves, *Geophys. Res. Lett.* **21**, 851-854.

78. Lee, L.C., Kan, J.R., and Akasofu, S.-I. (1985) On the origin of the cusp field-aligned currents, *J. Geophys.* **57**, 217-221.

79. Onsager, T.G. (1994) A quantitative model of magnetosheath plasma in the low latitude boundary layer, cusp and mantle, in J.A. Holtet and A. Egeland (eds.), *Physical signatures of magnetospheric boundary layer process*, Kluwer Academic Publishers, Dordrecht, pp. 385-400.

80. Zhou, X.-W. and Russell, C.T. (1997) The location of the high-latitude polar cusp and the shape of the surrounding magnetopause, *J. Geophys. Res.* **102**, 105-110.

81. Fung, S.F., Eastman, T.E., Boardsen, S.A., and Chen, S.-H. (1997) High-altitude cusp positions samples by the Hawkewe satellite, *Phys. Chem. Earth*, in press.

82. Sandahl, I., Lundin, R., Yamauchi, M., Eklund, U., Safrankova, J., Nemecek, Z., Kudela, K., Lepping, R.P., Lin, R.P., Lutsenko, V.N., and Sauvaud, J.-A. (1997) Cusp and boundary layer observation by INTERBALL, *Adv. Space Res.,* 20, 823-832.

83. Zhou, X.-W., Russell, C.T., Le, G., and Tsyganenko, N. (1997) Comparison of observed and model magnetic fields at high altitudes above the polar cap, *Geophys. Res. Lett.* **24**, 1451-1454.

84. Yamauchi, M. and Blomberg, L. (1997) Problems on mappings of the convection and on the fluid concept, *Phys. Chem. Earth*, 22, 709-714.

85. Yamauchi, M. (1997) Discussion 2: On the convection and velocity filter, *Phys. Chem. Earth*, 22, 607-608.